IChemE
www.ingentaselect.com/titles/02638762.htm
0263–8762/03/$23.50+0.00

Trans IChemE, Vol 81, Part A, February 2003

A STUDY OF BUBBLE VELOCITY AND BUBBLE RESIDENCE TIME IN A GASSED OSCILLATORY BAFFLED COLUMN
Effect of Oscillation Frequency

M. S. N. OLIVEIRA, A. W. FITCH and X. NI

Centre for Oscillatory Baffled Reactor Applications (COBRA), School of Engineering and Physical Sciences, Heriot–Watt University, Edinburgh, UK

In this paper, we report an experimental evaluation of velocity and residence time of single bubbles of different sizes in a gassed oscillatory baffled column (OBC) using a high-speed imaging technique. This work is particularly concentrated on the effect of oscillation frequency. The results show that the axial bubble velocities span several orders of magnitude with respect to the mean at an oscillatory frequency greater than 2 Hz. The ratio of the axial to radial bubble velocity components approaches unity at elevated oscillation frequencies. Combining the high-speed imaging with the high-resolution digital particle image velocimetry, we are able to examine the influence of the fluid flow on the bubble motion within the OBC. We also report the direct measurement of residence time of the bubbles within a baffled cell.

Keywords: oscillatory baffled column; bubble velocity; bubble residence time; high speed imaging; digital particle image velocimetry.

INTRODUCTION

Gas–liquid contacting is one of the most common operations used for mass transfer processes in chemical and biochemical applications. There have been many reports on this aspect in stirred tank vessels (Cooper *et al.*, 1944; Calderbank, 1959; Van't Riet, 1979; Smith *et al.*, 1977; Whitton and Nienow, 1993), airlift columns (Al-Qodah and Al-Hassan, 2000; Lewis and Davidson, 1985; Kawase and Hashiguchi, 1996; Chisti, 1989), bubble columns (Deckwer *et al.*, 1974; Grund *et al.*, 1992; Shah *et al.*, 1982; Heijnen and Van't Riet, 1984) and recently oscillatory baffled columns (Hewgill *et al.*, 1993; Ni and Gao, 1996a,b; Gao, 1996; Ni *et al.*, 1995a,b, 1997). The essential features in those operations are to break down sparged gas bubbles, air being one of the most used media, by means of different mixing mechanisms, into smaller and more uniform bubbles; and to increase the residence time of bubbles within a given device. The levels of dissolved oxygen in the aqueous medium can be measured directly using commercially available probes. In turn, this leads to the determination of mass transfer coefficients and subsequently an evaluation of the performance of the device. However, mass transfer measurements can not provide information on, for instance, bubble velocity, bubble residence time and bubble movement, and those elements are the main cause behind any mass transfer process. Consequently, research into the characteristics of bubbles in gas–liquid contractors has been extensive, including both experimental (Clift *et al.*, 1978; Deckwer, 1992) and numerical works (Clift *et al.*, 1978; Schlüter *et al.*, 1992; Deen *et al.*, 2001). Studies of this kind have been very difficult, given the fact that there is always a distribution in bubble sizes, and bubbles may break up or coalesce at any given time. Another added problem is that to capture quality images of bubbles at high aeration rate is still a challenging task. Traditionally, one has to rely on the information from single bubbles in order to interpret the behaviour of bubbles of a size distribution.

The velocity of a bubble in a continuous fluid is influenced by many physical parameters, such as density, viscosity and surface tensions of both gas and liquid, as well as by external effects, such as mixing conditions. Direct relationships between bubble terminal velocity and bubble size have been established in bubble columns (Clift *et al.*, 1978) and the typical dependence is shown in Figure 1 for pure water where D_{eq} is the equivalent bubble diameter (mm). From Figure 1 we see that for a small bubble (<1 mm in diameter) a steep increase in the bubble velocity with the bubble size is observed, indicating that small bubbles essentially behave as rigid spheres rising in a rectilinear path in a bubble column. Beyond a bubble diameter of around 1.3 mm, the velocity decreases with the bubble diameter. This is interpreted as bubbles of such sizes becoming large enough to allow shape deformations and increased drag for unsteady motion (Ford and Loth, 1998). Those bubbles travel a helical trajectory in a bubble column. In spite of the wide applicability of this type of relation, it is expected that bubbles rising in a highly

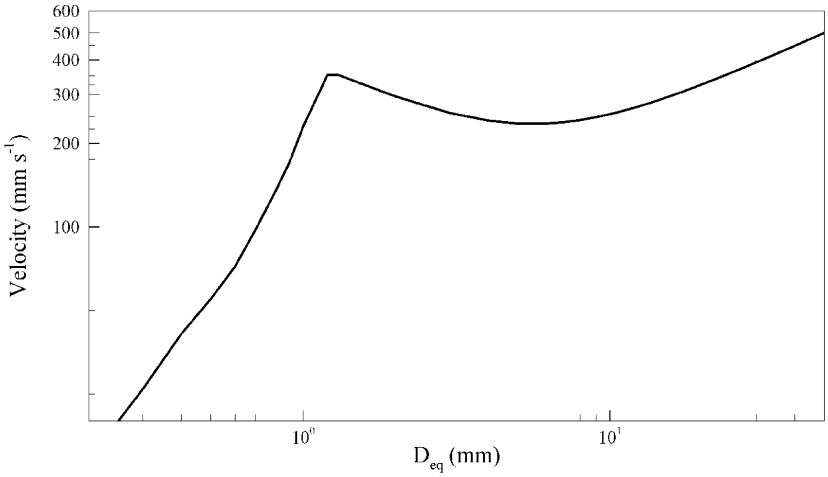

Figure 1. Terminal velocity of an air bubble rising in pure water versus equivalent bubble diameter (Clift *et al.*, 1978).

turbulent fluid will exhibit a more complex behaviour (Heijnen and Van't Riet, 1984).

The oscillatory baffled column (OBC) can be regarded as a new generation of bubble column (BC). Both columns are cylindrical and are operated in a batch mode, but the OBC incorporates equally spaced orifice baffles together with fluid oscillation, providing a significantly different flow pattern compared with the BC. The OBC's simple operating mechanism can be understood with the help of Figure 2. Fundamentally, sharp edges (provided by the baffles) must be present transverse to a fully reversing flow. The interactions between baffles and the oscillating fluid generate significant eddy motion in both axial and radial directions, offering uniform and enhanced mixing within each baffled cavity as well as along the length of the column.

There are four dimensionless groups that govern the fluid mechanical conditions in the OBC: the baffle spacing ($H = L/D$) and the baffle free area [$\alpha = (D_{\text{orifice}}/D)^2$], which are kept constant in this study; the oscillatory Reynolds number (Re_o) and the Strouhal number (St), defined as:

$$Re_o = \frac{2\pi f x_o \rho D}{\mu} \tag{1}$$

$$St = \frac{D}{4\pi x_o} \tag{2}$$

where L is the axial length between baffles (m), D is the diameter of the column (m), D_{orifice} is the diameter of the baffle's orifice (m), ρ is the fluid density (kg m^{-3}), x_o is the oscillation amplitude (m, centre to peak), f is the oscillation frequency (Hz) and μ is the fluid viscosity (kg m^{-1} s^{-1}). The oscillatory Reynolds number describes the intensity of mixing applied to the column, while the Strouhal number is the ratio of column diameter to stroke length, characterizing the effective eddy propagation (Ni and Gough, 1997; Mackley and Ni, 1991; Howes, 1988; Ni *et al.*, 1998).

It is a fact that there are fundamental differences of fluid mechanics between the OBC and the bubble column, and this has resulted in a number of advantages of the OBC over the traditional bubble column in mass transfer performance (Hewgill *et al.*, 1993). To understand bubble behaviours in an OBC, we present, in this paper, the results of our research into bubble movement, velocity and residence time of single bubbles of different sizes within an OBC.

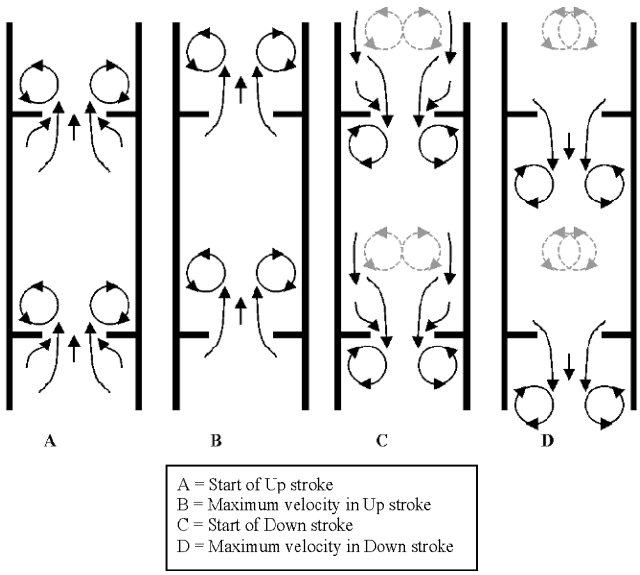

Figure 2. Mechanism of mixing in an oscillatory baffled column.

EXPERIMENTAL SET UP AND PROCEDURE

The Oscillatory Baffled Bubble Column

The batch OBC used in this study is made of a vertical Perspex tube of 500 mm in height and 50 mm in diameter with a liquid capacity of 1 l, as shown in Figure 3. Six baffles, each with an orifice diameter of 23 mm and evenly spaced 75 mm apart, are connected by two connecting rods. A rectangular viewing box is sealed around the tube at the point of investigation and filled with water to minimize refractive effects caused by wall curvature. A stainless steel bellows, flanged onto the base of the column and connected with the fly arm of an electric motor, drives the oscillation and the speed of the motor provides oscillation frequencies between 0.2 and 10 Hz. The eccentric distance between the

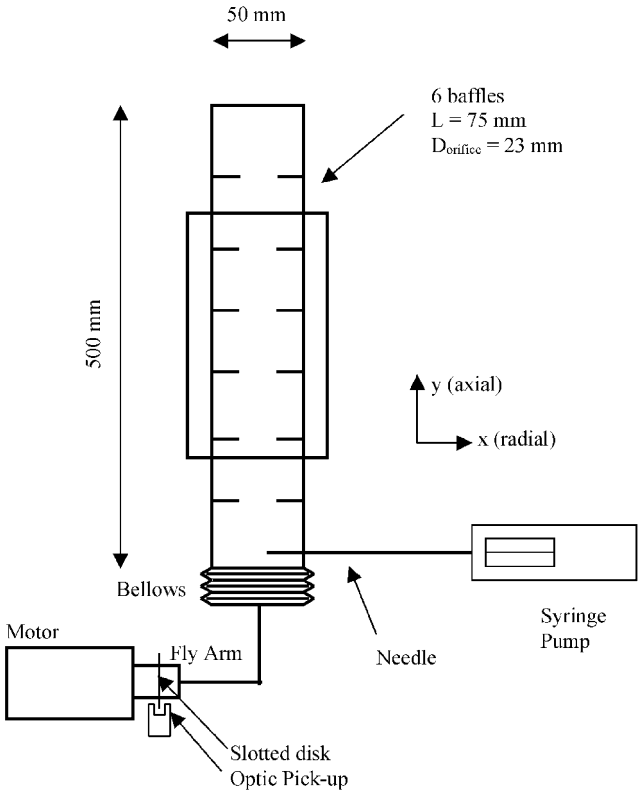

Figure 3. An oscillatory baffled column.

fly arm and the crank of the motor generates oscillation amplitudes of 2–8 mm (centre to peak). In this study into the effect of oscillatory frequency, the amplitude was fixed at 4 mm. Affixed to the fly arm is a thin slotted disc that revolves with the motor through an optic pick-up, which generates a pulse at every peak of oscillation. This pulse is important as it provides a mechanism to synchronize the peak of oscillation with the start of the high-speed camera operation. Air is supplied by a Labotron syringe pump via a septum at the base of the column where needles of different sizes can be fitted to the centre of the column in order for single bubbles of various sizes to be generated.

Set-Up of the High-Speed Imaging

The high-speed imaging set-up is shown in Figure 4. A high-speed mono coloured CCD camera (Kodak Ektapro 4540mx) is operated at a frame rate of 500 frames per second and triggered to record images at the start of the oscillation. The camera has a 256×256 CCD pixel array. A white light source is situated behind the column directed towards the camera silhouetting the bubbles. Between the light source and the column is a filter sheet to standardize the light giving sharper and uniform images. Linked to the memory of the camera is a play back monitor to view images and a PC to download images (as TIFF).

Experimental Procedure

The OBC is filled with 1 l of deionised water, the operating conditions are set and the trigger switch is set to open. The camera starts to record upon receiving a trigger pulse at the peak of an arbitrary oscillation cycle as aforementioned. The recorded sequence is viewed on the play back monitor and downloaded to the PC. Note that the crucial timing information is tagged with each file. The procedure is repeated in an OBC for oscillating frequencies of 0, 1, 2 and 4 Hz and at a fixed oscillating amplitude of 4 mm (centre to peak); as well as in a traditional bubble column (i.e. the same column with no baffles and no oscillation).

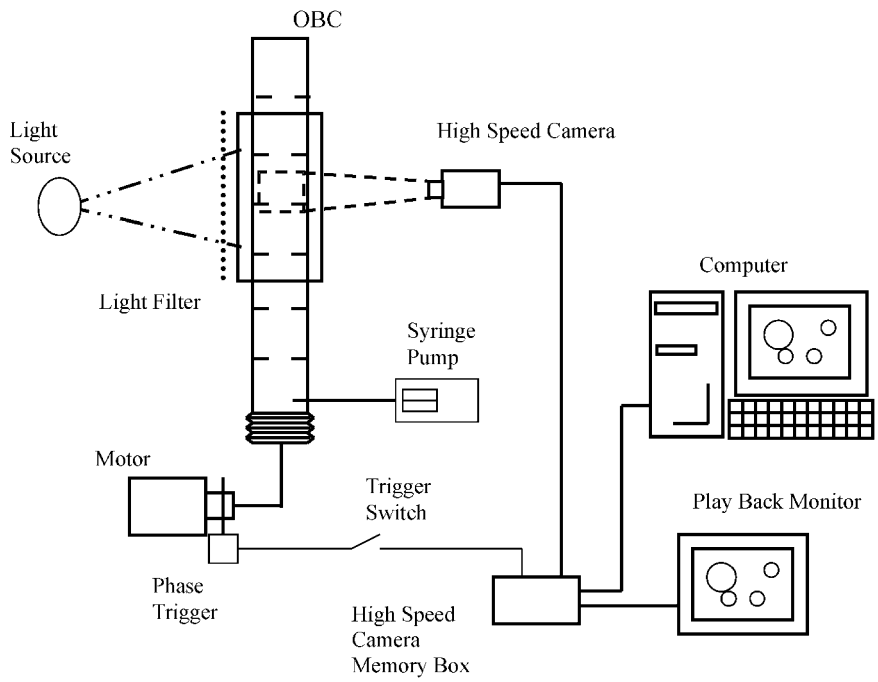

Figure 4. A schematic diagram of the OBC and high-speed imaging set-up.

	Scenario 1	Scenario 2	Scenario 3
Pictorial Movement	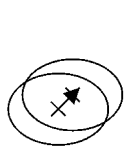	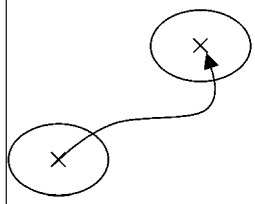	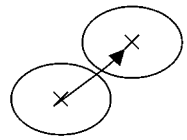
Symptoms	Too few pixels between bubble centre points	Good number of pixels between centre points	Good number of pixels between centre points
Diagnosis	Motion is direct	Motion is too indirect	Motion is direct enough

Figure 5. Possible bubble displacements.

BUBBLE VELOCIMETRY

To determine the instantaneous velocity of the bubble the basic equation: speed = distance/time, is utilized. The timing information is known since every consecutive image is 2 ms apart (the reciprocal of the frame rate) and the displacement can be evaluated by measuring and comparing the positions of a bubble's centre of gravity in two consecutive images. A built-in function of the Aequitas image analysis software is used to determine the centre positions of the bubble and also its size, measured as the projected two-dimensional area. The bubble size is then converted to a diameter (D_{eq}), equivalent to a sphere with the same projected area. The displacements, and thus the velocities, in both the x and y directions (as shown in Figure 3) can be determined. For accurate velocimetry there must be an appreciable displacement and direct bubble movement between images. Figure 5 shows three possible scenarios each showing a movement of a single bubble with a different time separation. In Scenario 1 there are too few pixels of separation between the centre points of the bubble to identify the distance. On the other hand, if the bubbles are too far apart, the displacement of the bubble might not be in a straight line, yielding an incorrect value for the determination of the instantaneous velocity—Scenario 2. Scenario 3 is

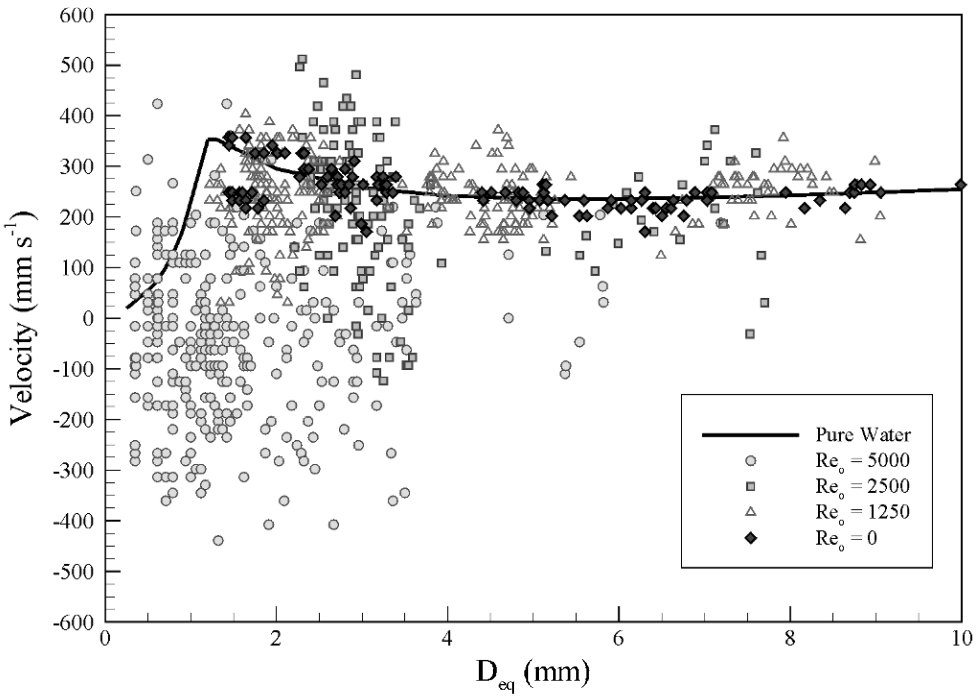

Figure 6. Instantaneous axial velocity of bubble vs equivalent bubble diameter with predicted bubble terminal velocities (Clift *et al.*, 1978) superimposed.

Table 1. Oscillatory velocity for range of experimental conditions.

f (Hz)	Re_o	$2\pi f x_o$ (mm s^{-1})
0 or BC	0	0
1	1250	25
2	2500	50
4	5000	100

the ideal one with both a direct pathway and noticeable bubble movement. To obtain a trajectory similar to Scenario 3 in Figure 5 a separation between the bubble images of up to 10 frames is often required (where 10 frames correspond to 20 ms). The information is captured over a fixed area within one baffled cell, which means that a 1 mm × 1 mm area contains about 3 × 3 pixels. Due to the size and velocity of the bubbles compared with the total size of interrogation area (one baffled cell), we felt that the resolution was more than adequate. In order to eliminate significant bubble–bubble interactions, only images containing single bubbles were analysed. This was readily accomplished in our study except at the highest oscillation frequency of 4 Hz, for example, multiple bubbles were in the field of view at any given time. Under these conditions, an individual bubble was tracked and analysed, images containing bubbles overlapping, coalescing or breaking were disregarded from analysis.

Figure 6 plots the instantaneous axial velocity of bubbles, U_y, against the equivalent diameter of bubbles at a fixed oscillation amplitude of 4 mm, for oscillatory frequencies of 0, 1, 2 and 4 Hz. Note that, since all other variables in equation (1) are fixed, the oscillatory Reynolds number (Re_o) becomes directly proportional to the oscillation frequency. Table 1 shows the corresponding Re_o and the

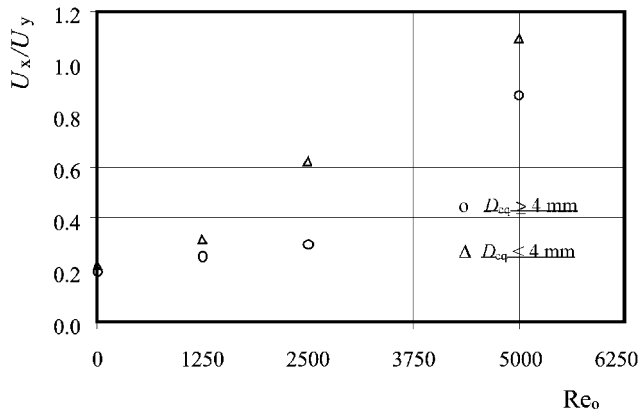

Figure 8. Effect of frequency on the ratio of radial and axial components of the velocity for bubbles with different sizes.

fluid oscillatory velocity ($2\pi f x_o$) for these four frequencies. The solid line in Figure 6 represents the terminal velocity of an air bubble rising in pure water (Clift *et al.*, 1978). When there is no oscillation in the baffled column, the trend of the bubble velocities (legend for $Re_o = 0$) is well in line with the literature prediction. On the introduction of fluid oscillations, we observe a wide scatter of bubble velocities both above and below the theoretical line (solid line), with the values of the velocity spanning several orders of magnitude. When the oscillation frequency is increased above 2 Hz ($Re_o = 2500$) one striking feature is apparent: the negative bubble velocities, caused by the oscillatory motion, increase significantly in both number and magnitude. As will be seen later, this is a key factor in the increase of bubble residence time in the column. It should be noted that it is very difficult to obtain images containing large bubbles at high oscillation frequencies, as they are unsteady and prone to break up under such operating

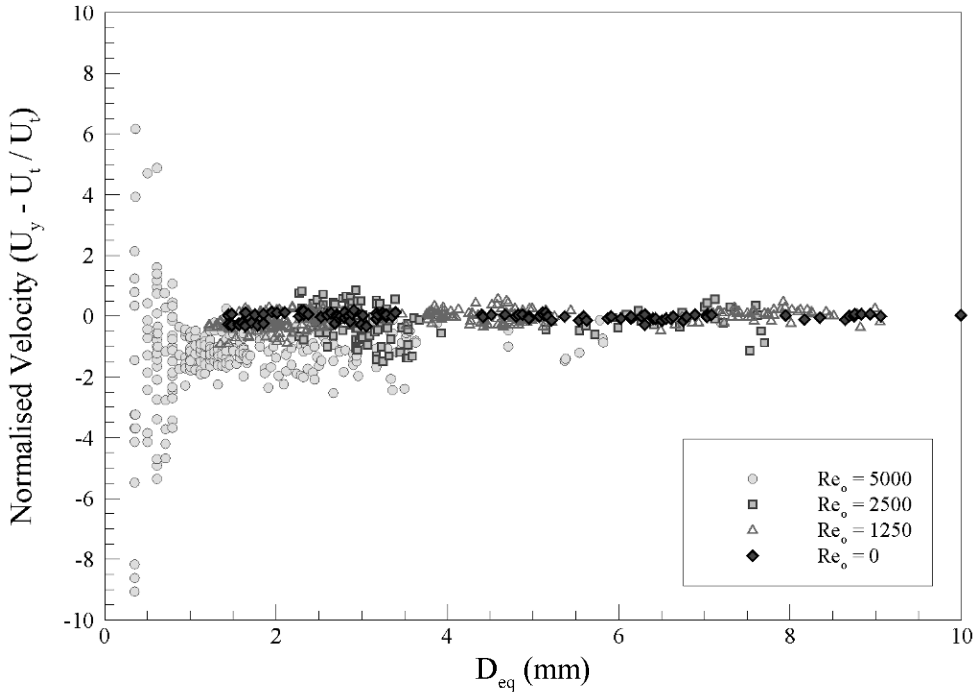

Figure 7. Instantaneous bubble velocity normalized with terminal velocity vs equivalent bubble diameter.

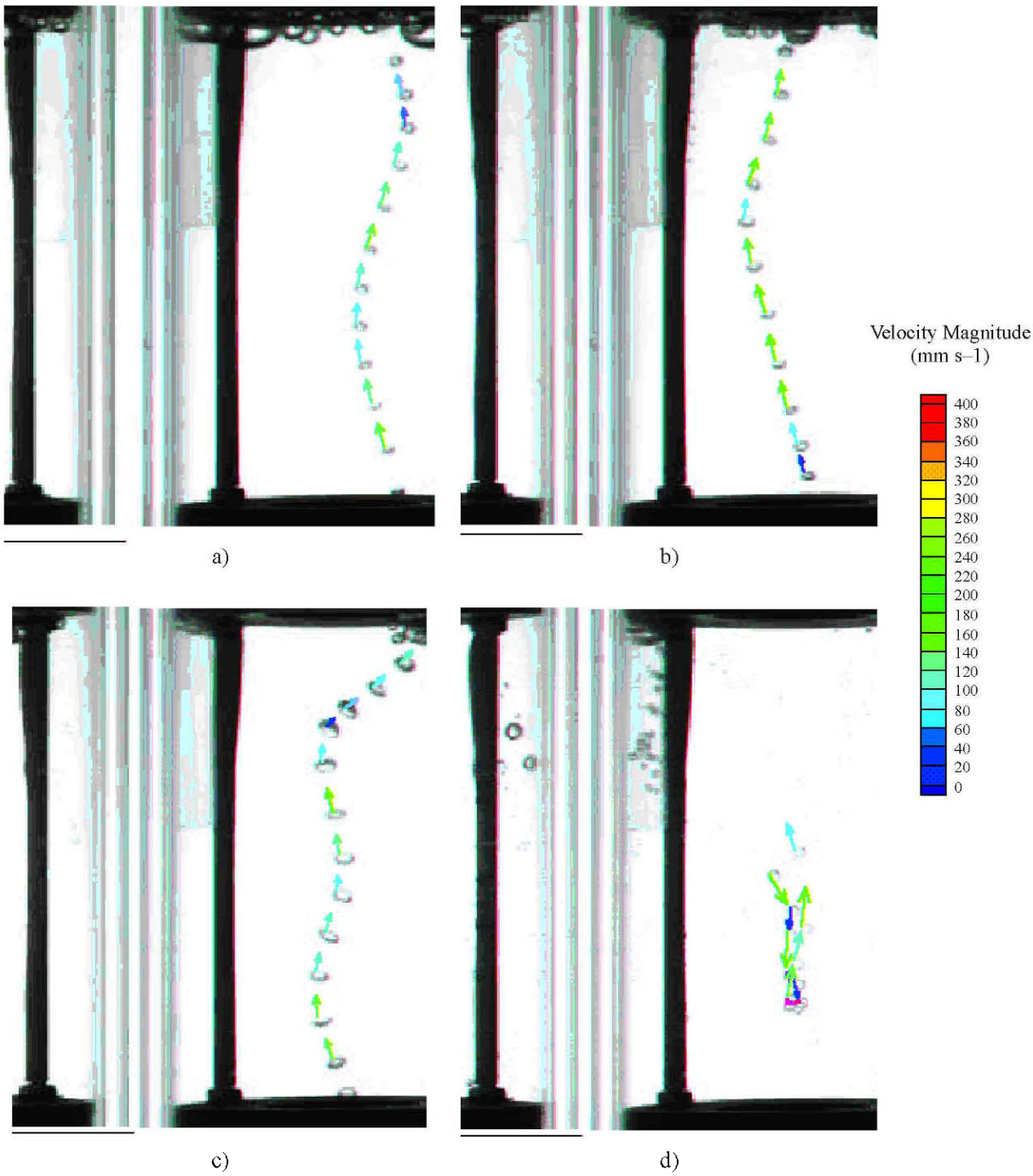

Figure 9. Motion and velocity of single bubble: (a) with no oscillation; (b) at $Re_o = 1250$, $St = 1.0$ ($x_o = 4$ mm, $f = 1$ Hz); (c) at $Re_o = 2500$, $St = 1.0$ ($x_o = 4$ mm, $f = 2$ Hz); (d) at $Re_o = 5000$, $St = 1.0$ ($x_o = 4$ mm, $f = 4$ Hz).

conditions. Consequently, for high frequencies, relatively few bubbles analysed here have diameters of greater than 4 mm.

If we denote the velocity of the trend-line (solid line) as the terminal velocity, U_t, we can replot data in Figure 6 as $(U_y - U_t)/U_t$ vs D_{eq} in Figure 7, where the zero line $[(U_y - U_t)/U_t = 0]$ indicates the terminal velocity predictions, shown in Figure 1. It is clear that the span of the increase in the normalized velocity is remarkable on the introduction of baffles and oscillation.

In our current set up, we are also able to separate the instantaneous velocities of single bubbles into both axial

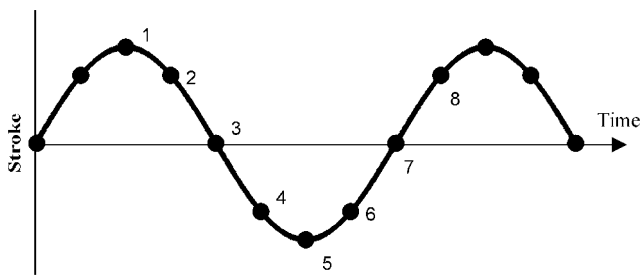

Figure 10. Phase position with respect to time.

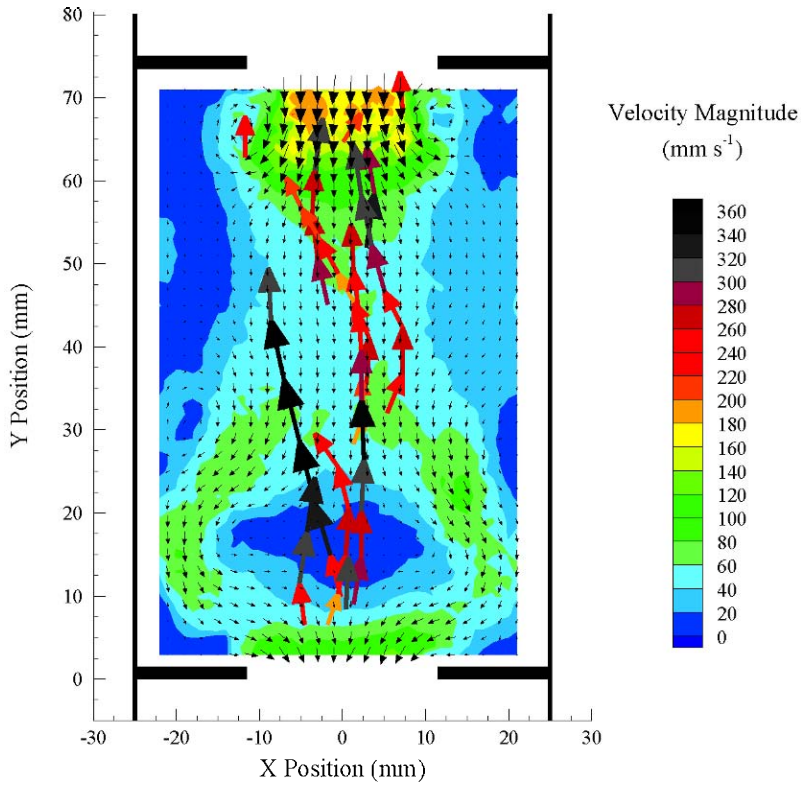

Figure 11. Velocity of single bubbles superimposed onto fluid flow vector map at phase 3. $Re_o = 1250$, $St = 1.0$ ($x_o = 4$ mm, $f = 1$ Hz).

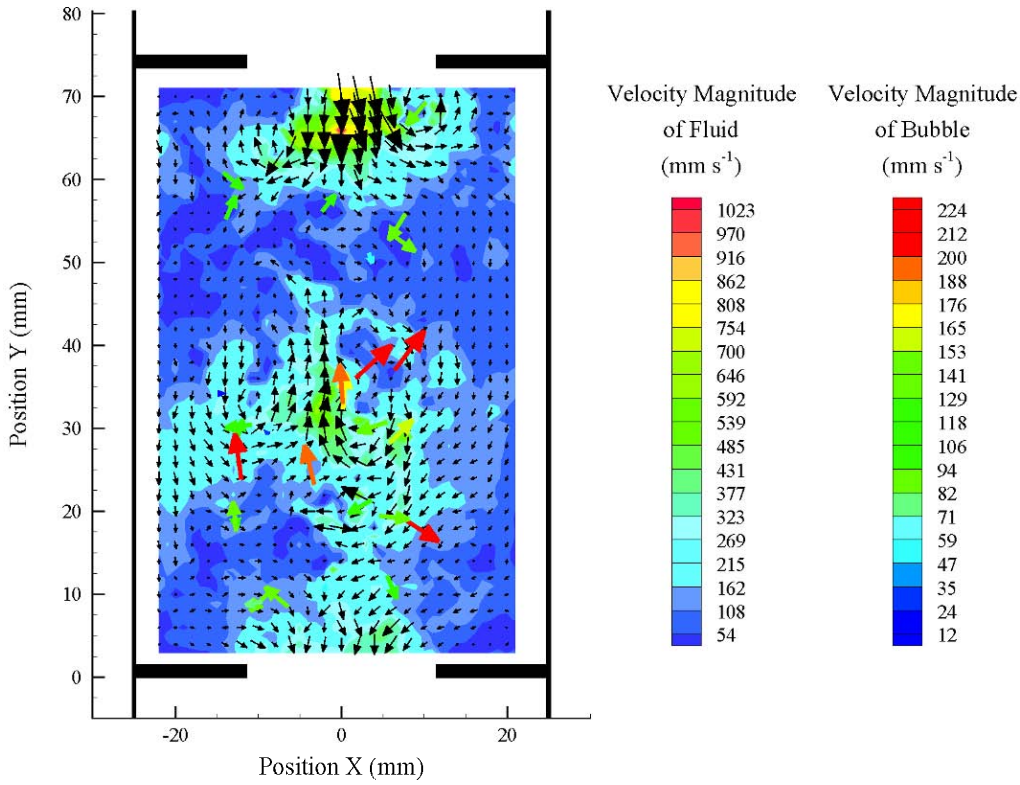

Figure 12. Velocity of bubbles superimposed onto fluid flow vector map at phase 3. $Re_o = 5000$, $St = 1.0$ ($x_o = 4$ mm, $f = 4$ Hz).

(U_x) and radial (U_y) components. Figure 8 shows the ratio between the U_x and U_y components as a function of Re_o. Clearly, if this ratio equals one, this means that the bubble moves equally in both x and y directions. When no oscillation is applied to the OBC, the ratio is about 0.2 (the axial motion is five times greater than the radial one). With the presence of fluid oscillation, the velocity ratio for the smaller bubbles ($D_{eq} < 4$ mm) shows an almost linear rise from 0.2 to 1.1 as the Re_o increases to 5000. For the large bubbles, the velocity ratio remains more or less unchanged until the highest frequency ($Re_o = 5000$). This confirms the fact that the bubbles in the OBC, especially smaller ones, are strongly influenced by the oscillations.

By linking a series of consecutive bubble images it is possible to show the trajectory of a bubble as it rises through the column. We have used the Adobe PhotoShop to layer about 15 images together into a single file. For better clarity, only cases in which there is no overlap between bubbles in consecutive images are selected. Figures 9(a)–(d) show the pathway of a single bubble in a baffled cell at an oscillation frequency of 0, 1, 2 and 4 Hz respectively. Superimposed onto these images are the velocity vectors of the bubble at each point in time. From these figures we see that as the oscillation frequency increases there is a greater disturbance in the bubble's pathway, manifested by a change in direction of the velocity vectors. At a frequency of 2 Hz [Figure 9(c)] the descending fluid holds up the bubbles near to the top baffle. At a frequency of 4 Hz [Figure 9(d)] the pathway of the bubble displays a complete U-shape format. This will have significant impact on the residence time of bubbles. Note that the single bubble in Figure 9(d) has been isolated from the surrounding bubbles for the purposes of visual clarity. Another definitive feature of these figures is that as the frequency increases the amount of bubbles trapped below the upper baffle decreases. Understandably, the mixing intensity brought about by an increase in the oscillation frequency overcomes the surface attraction forces of the baffles and leaves no room for the bubble to settle. This will be discussed further in the next section.

In our previous studies, we have reported direct measurements of fluid velocity within the OBC using a high-resolution digital particle image velocimetry (DPIV) system. The details of this work can be found elsewhere (Ni *et al.*, 2002). Due to the oscillation, the fluid is displaced sinusoidally with time, and the fluid velocities can be measured at eight phases of an oscillation cycle, as shown in Figure 10. Observations suggest that on the up stroke (phases 5–8) bubble velocities would increase, whereas on the down stroke (phases 1–4) bubbles are generally held up. To investigate the effect that the fluid flow and its velocity have on the velocity and direction of the bubble we superimpose DPIV fluid velocity vector maps (obtained in the absence of bubbles) with the bubble velocities and their positions, determined using the high speed video camera. Phase 3, which corresponds to the maximum velocity of the down stroke, was selected as a typical example. Figures 11 and 12 show the results at phase 3 for $St = 1.0$, and $Re_o = 1250$ and $Re_o = 5000$, respectively, where the coloured arrows denote bubble velocity vectors. It can be seen that at $Re_o = 1250$ (Figure 11) the bubbles attempt to follow the regions where the fluid flow is upwards and try to avoid the fluid elements of negative velocity, carving well defined pathways along the bulk phase. At $Re_o = 5000$ (Figure 12), however, the appearance of the bubble velocity vectors along the baffled cell is rather chaotic. This is due to the highly turbulent and irregular flow patterns under these operating conditions. The scattered bubble velocity vectors reflect the vortical nature of the fluid flow. It should be mentioned that the velocity scale of the bubble is different from that of the fluid in Figure 12; this is because the velocities of the bubbles were considerably smaller than that of the fluid.

BUBBLE RESIDENCE TIME

The bubble residence time is a simple concept describing the length of time a bubble resides in a baffled cell of the OBC. It is calculated by subtracting the time at which the bubble enters the cell through the lower baffle, from the time at which it exits through the upper baffle. The times are determined within 2 ms, by viewing the bubble motion on the play back monitor of the high-speed imaging set up.

There are generally two noticeable behaviours for a bubble to travel when passing through a cell in the OBC, which leads to two types of bubble residence time. The first case is when a bubble enters and leaves the cell without obstruction. In the second case, a bubble enters the cell, and then nests below a baffle, e.g. at lower frequencies of oscillation, before being swept back into the flow and ultimately departing the cell. We therefore introduce the concepts of a real and an apparent residence time of bubbles. The real residence time is the time taken for a bubble to enter and leave a cell, regardless of its pathway. The apparent residence time is the time taken for a bubble to enter and then reach the upper baffle without leaving the cell. The difference between the two residence times will provide an estimate of the time that a bubble remains trapped beneath the baffle. For high oscillation frequencies such a phenomenon is negligible. However, at lower oscillation intensities there is a very significant difference between the apparent and real residence times, which is in fact a unique feature in the OBC. Figure 13 illustrates a comparison between the two residence times for an oscillatory Reynolds number of 2500. The data were divided into three separate classes, according to the diameters of the tracked bubbles. By examining the results, two main features are readily observed. Firstly, both residence times decrease with

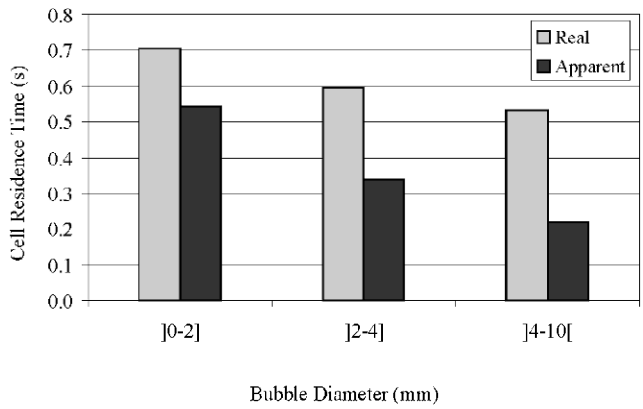

Figure 13. Real and apparent bubble residence times at $Re_o = 2500$, $St = 1.0$ ($x_o = 4$ mm, $f = 2$ Hz).

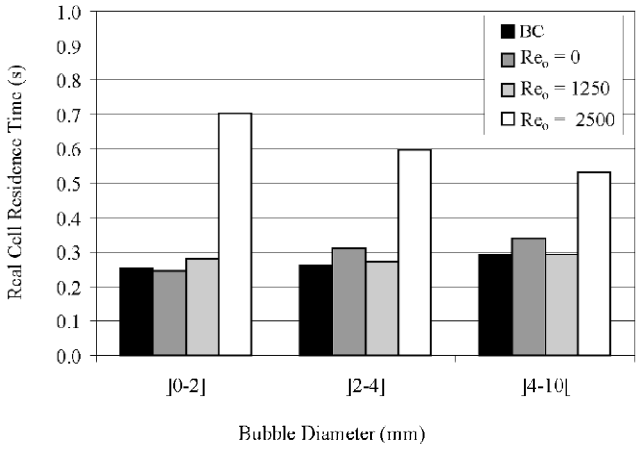

Figure 14. Real bubble residence times for different bubble classes.

the increase of bubble size. This is within our expectation. Secondly, the rate of decrease in the real residence time is significantly less than that in the apparent residence time, which evidences the retention of more large bubbles nesting beneath the baffles. It would have two major effects in gas–liquid contacting processes: to increase the residence time of the bubble and to promote bubble coalescence and subsequent breakage, both of which are beneficial to the overall mass transfer processes. Such information provides us with the insight of bubble movement within an OBC, and the identification of the bubble nesting time would allow us to examine its individual contribution to the overall mass transfer in the future.

Figure 14 shows the measured bubble (real) residence time for a bubble column and the OBC at the frequencies of 0, 1 and 2 Hz ($Re_o = 0$–2500), and for the three classes of bubble size. For the case of the bubble column, where there are no cells, the bubble residence time is thus defined as the time for a bubble to travel the equivalent length of the cell. From Figure 14, the general trend is that the residence times of bubbles remain more or less the same in the absence of oscillation and at the lower oscillation conditions. Under those circumstances, the contribution of residence times of bubbles to the overall mass transfer performance would be of little difference for the two types of systems. At high oscillatory conditions, on the other hand, the average residence times of all three classes of bubbles are doubled as compared with the rest. The contribution of the residence time of the bubble to the overall gas–liquid contacting processes is thus significant in these conditions. Note that it was not possible to accurately obtain the residence time of bubbles at frequencies above 2 Hz, due to the presence of multiple bubbles in the field of view and the data shown in Figure 14 are our best estimates.

CONCLUSION

We have shown in this paper the detailed motion of single bubbles of different sizes travelling along an oscillatory baffled column using the high-speed camera. The vivid pictures and graphs indicate the vortical nature of the oscillating flow, which has a number of advantages over the traditional bubble column, such as much longer bubble residence times and much more complex velocity profiles. We also identified, in the study of residence time of bubbles, the unique feature of bubble nesting beneath a baffle plate at lower oscillating conditions. This information can be used in the interpretation of the enhanced mass transfer rates found in this type of geometry.

NOMENCLATURE

D	column internal diameter, m
D_{eq}	equivalent diameter defined as diameter of a circle having the same area as the projected area of the bubble, m
$D_{orifice}$	baffle orifice diameter, m
F	frequency of oscillation, Hz
H	baffle spacing
L	axial length between baffles, m
Re_o	oscillatory Reynolds number as defined in equation (1)
St	Strouhal number as defined in equation (2)
U_t	bubble terminal velocity, m s^{-1}
U_x	'radial' component of the bubble velocity, m s^{-1}
U_y	axial component of the bubble velocity, m s^{-1}
x_o	amplitude of oscillation, m

Greek symbols

α	baffle free area
ρ	fluid density, kg m^{-3}
μ	fluid viscosity, kg m^{-1} s^{-1}

REFERENCES

Al-Qodah, Z. and Al-Hassan, M., 2000, Phase holdup and gas-to-liquid mass transfer coefficient in magneto stabilized g-l-s airlift fermenter, *Chem Engng J*, 79: 41–52.

Calderbank, P.H., 1959, Physical rate processes in industrial fermentation. Part ii: Mass transfer coefficients in gas–liquid contacting with and without mechanical agitation, *Trans IChemE*, 37: 173–185.

Chisti, M.Y., 1989, *Airlift Bioreactors* (Elsevier Science, Amsterdam, The Netherlands).

Clift, R., Grace, J.R. and Weber, M.E., 1978, *Bubbles, Drops, and Particles*, Chap. 7 (Academic Press, London, UK), pp 168–201.

Cooper, C.M., Fernstrom, G.A. and Miller, S.A., 1944, Performance of agitated gas–liquid contactors, *Ind Engng Chem*, 36: 504–509.

Deckwer, W.D., 1992, *Bubble Column Reactors* (Wiley, Chichester, UK).

Deckwer, W.D., Burckhart, R. and Zoll, G., 1974, Mixing and mass transfer in tall bubble columns, *Chem Engng Sci*, 29: 2177–2188.

Deen, N.G., Solberg, T. and Hjertager, B.H., 2001, Large eddy simulation of the gas–liquid flow in a square cross-sectioned bubble column, *Chem Engng Sci*, 56: 6341–6349.

Ford, B. and Loth, E., 1998, Forces on ellipsoidal bubbles in a turbulent shear layer, *Phys Fluids*, 10: 178–188.

Gao, S., 1996, *Characterisation of pulsed baffled reactors*, Ph.D. thesis (Strathclyde University, UK).

Grund, G., Schumpe, A. and Deckwer, W.D., 1992, Gas–liquid mass transfer in a bubble column with organic liquids, *Chem Engng Sci*, 47: 3509–3516.

Heijnen, J.J. and Van't Riet, K., 1984, Mass transfer, mixing and heat transfer phenomena in low viscosity bubble column reactors, *Chem Engng J*, 28: B21–B42.

Hewgill, M.R., Mackley, M.R., Pandit, A.B. and Pannu, S.S., 1993, Enhancement of gas–liquid mass transfer using oscillatory flow in a baffled tube, *Chem Engng Sci*, 48: 799–809.

Howes, T., 1988, *On the dispersion of unsteady flow in baffles tubes*, Ph.D. thesis (The University of Cambridge, Cambridge, UK).

Kawase, Y. and Hashiguchi, N., 1996, Gas–liquid mass transfer in external-loop airlift columns with newtonian and non-newtonian fluids, *Chem Engng J*, 62: 35–42.

Lewis, D.A. and Davidson, J.F., 1985, Mass transfer in a recirculating bubble column, *Chem Engng Sci*, 40: 2013–2017.

Mackley, M.R. and Ni, X., 1991, Mixing and dispersion in a baffled tube for steady laminar and pulsatile flow, *Chem Engng Sci*, 46: 3139–3151.

Ni, X. and Gao, S., 1996a, Scale-up correlation for mass transfer coefficients in pulsed baffled reactors, *Chem Engng J*, 63: 157–166.

Ni, X. and Gao, S., 1996b, Mass transfer characteristics of a pilot pulsed baffled reactor, *J Chem Tech Biotechnol*, 65: 65–71.

Ni, X. and Gough, P., 1997, On the discussion of the dimensionless groups governing oscillatory flow in a baffled tube, *Chem Engng Sci*, 52: 3209–3212.

Ni, X., Gao, S. and Pritchard, D.W., 1995a, A study of mass transfer in yeast in a pulsed baffle bioreactor, *Biotech Bioengng*, 45: 165–175.

Ni, X., Gao, S., Cumming, R.H. and Pritchard, D.W., 1995b, A comparative study of mass transfer in yeast for a batch pulsed baffled bioreactor and a stirred tank fermenter, *Chem Engng Sci*, 50: 2127–2136.

Ni, X., Gao, S. and Santangeli, L., 1997, On the effect of surfactant on mass transfer to water-glycerol solutions in a pulsed baffled reactor, *J Chem Tech Biotechnol*, 69: 247–253.

Ni, X., Brogan, G.A.S., Bennett, D.C. and Wilson, S.F., 1998, A systematic study of the effect of geometrical parameters on mixing time in oscillatory baffled columns, *Trans IChemE, Part A, Chem Eng Res Des*, 76: 635–642.

Ni, X., Jian, H. and Fitch, A.W., 2002, Cfd modelling of flow patterns in an oscillatory baffled column, *Chem Engng Sci*, 57: 2849–2862.

Schlüter, S., Steiff, A. and Weinspach, P.-M., 1992, Modeling and simulation of bubble column reactors, *Chem Engng Process*, 31: 97–117.

Shah, Y.T., Kelkar, B.G., Gobole, S.P. and Deckwer, W.D., 1982, Design parameter estimations for bubble column reactors, *AIChemE J*, 28: 353.

Smith, J.M., Van't Riet, K. and Middleton, J.C., 1977, Scale up of agitated gas–liquid reactors for mass transfer, *Proceedings of 2nd European Conference on Mixing*, Cranfield, F4, pp 51–68.

Van't Riet, K., 1979, Review of measuring methods and results in non viscous gas–liquid mass transfer in stirred vessels, *Ind Engng Chem Process Des Devl*, 18: 357–364.

Whitton, M.J. and Nienow, A.W., 1993, Scale up correlations for gass hold up and mass transfer coefficients in stirred tank reactors, *3rd International Conference on Bioreactor and Bioprocess Fluid Dynamics*, pp 135–149.

ACKNOWLEDGEMENTS

The authors wish to acknowledge EPSRC, Fundação para a Ciência e Tecnologia and Heriot–Watt University for the financial support.

ADDRESS

Correspondence concerning this paper should be addressed to Professor X.-W. Ni, School of Engineering and Physical Sciences, Chemical Engineering, Heriot–Watt University, Edinburgh EH14 4AS, UK.
E-mail: x.ni@hw.ac.uk

The manuscript was received 11 March 2002 and accepted for publication after revision 1 November 2002.